On a 2D zoom for 1D shallow-water model: coupling and data assimilation

Jerome Monnier, Igor Gejadze

On a 2D 'zoom' for the 1D shallow water model: coupling and data assimilation

I.Yu. Gejadze [a,1,*] J.Monnier [b,1]

[a] *Department of Civil Engineering, University of Strathclyde, John Anderson Building 107 Rottenrow, Glasgow, G4 0NG, UK*

[b] *LJK - MOISE project-team, INP-Grenoble, France*

Abstract

In the context of river hydraulics we elaborate the idea of a 'zoom' model locally superposed on an open-channel network global model. The zoom model (2D shallow water equations) describes additional physical phenomena, which are not represented by the global model (1D shallow water equations with storage areas). Both models are coupled using the optimal control approach when the zoom model is used to assimilate local observations into the global model (variational data assimilation) by playing the part of a mapping operator. The global model benefits from using zooms, while no substantial modification to it is required. Numerical results on a toy test case show the feasibility of the suggested method.

Key words: zoom model, coupling, optimal control, variational data assimilation, shallow water equations, flood modeling
PACS:

1 Introduction

Operational hydrological models that describe a watershed as a network of open channels are presently based on the 1D St-Venant equations (or shallow water equations (SWE)) with storage areas. Sometimes, these models are called 1.5D river models, see e.g. [5]. The main advantage of these models is the low computational

* Tel: +44 0 (141) 548-4773; fax: +44 0 (141) 553-2066
Email addresses: igor.gejadze@strath.ac.uk, Jerome.Monnier@imag.fr (J.Monnier).

[1] This study has been co-funded by Région Rhône-Alpes (project "numerical prevention for floods")

cost that allows nearly real time analysis of large-scale river network models that is required for decision-making. The storage areas (static volumes which may store water, such as flood plains for example) are modeled in the 1D model by source terms which are evaluated using empirical expressions, [5]. The flow dynamics inside storage areas are not modeled.

Since the 2D flow pattern inside a given storage area may be of interest, we seek to superpose a local 2D SWE model to the 1.5D open-channel network global model. This may also improve the accuracy of source terms used in the 1.5D model formulation. Another reason to superpose local 2D zoom models arises in the context of data assimilation (DA). Calibration of hydraulic river models can be difficult to achieve in practice. Unknown parameters can be the inflow discharge, the initial condition or the Manning coefficient. Variational data assimilation can be an efficient method of calibrating these models, see e.g. [16], [2], [14], [9]. In general, the variables of the 1D model are the wet cross-section area and the corresponding volumetric discharge, while the measured physical quantities are the local surface elevation and velocities. A correspondence between the 1D variables and measured local values is approximate at best. However, these local measured values could naturally be the variables of a local 2D SWE model. In the present study we assimilate data measured inside a 2D zoom area (for example, elevation) into the 1D network model and couple both models within the same optimal control loop.

It is possible to introduce local 2D models into a 1.5D network model using the domain decomposition method (DDM). This produces a set of 1D channels and 2D areas, see e.g. [6],[17]. The coupling techniques which could be applied in this case vary from the classical Schwarz method with overlapping, the wave-form relaxation method (WFR) [15], [8] (which is a subset of the global time Schwartz method), and methods based on optimal control [11].

We suggest the use of a coupling principle which may be called 'superposition' rather than decomposition. The key point is that we keep the existing 1.5D model intact, but source terms within the area of interest are estimated via the solution of a superposed 2D local model as 'defect corrections' [4]. The 1D model, in turn, provides a basis for estimation of the boundary conditions (BC) at open boundaries of each 2D area.

In oceanography, the arrangement of a local (normally finer mesh) model superposed on a global (coarse mesh) model, with the two models interacting for mutual benefit, is called two-way nesting, see e.g. [7]. These models, however, are usually based on the same equations (they model the same physics). In our case the local model is a richer model since it includes extra physical phenomena which do not exist in the global model. We shall call such a model a zoom model, which stands for 'a two-way nested richer local model'. The proposed arrangement is convenient because the 1.5D-network model remains intact and can communicate to the 2D zooms via the source term, thus one can use available standard software (if the adjoint of the 1.5D model has been generated).

A possible difficulty with the proposed superposition method is that the models are not consistent. That is:

a) the 1D model cannot provide the full set of BC for the 2D 'zoom' model;

b) the 1D model is usually solved on much coarser mesh with typical ratio of 10^1-10^2 for the space mesh size and 10^2-10^3 for the time step between 2D and 1D models. The problems related to the inconsistency could be overcome if we couple models using optimal control.

In the present study, first we build the coupling procedure based on the WFR method for which the 1D and 2D zoom models are solved consecutively in the global time domain, exchanging information between completed runs. To provide a sufficient set of BC for the 2D 'zoom' model we must use additional assumptions. Numerical experiments show efficiency of the method for the case when the 2D flow at the boundaries of the 'zoom' model exhibits essentially 1D behavior.

Then, we turn to the issue of variational data assimilation, assuming data are available within the zoom area. The key idea is to build a joint assimilation-coupling procedure (JAC), which solves simultaneously both DA and coupling problems, rather than the classical DA problem for the already coupled model (obtained using WFR, for example). To this end, we specify an extended cost functional such that in addition to the usual DA terms (misfit between model predictions and measured data), it includes coupling conditions written in a weak integral form. The main advantage of this approach is that no additional assumptions are needed, i.e. one can evade the usual difficulties of coupling inconsistent models. Information extracted from data measured within the zoom area not only allows gaps in the coupling conditions to be filled in, but also propagates into the 1.5D model and so enables its parameters to be identified, for example BC at the ends of the 1D section.

The extended cost functional is minimized using the quasi-Newton L-BFGS algorithm, [12], while the gradient is computed using the adjoint method. Numerical experiments show that the JAC algorithm must be equally or less expensive compared to the DA procedure for the coupled model. In the numerical tests conducted, we consider a toy flooding event that involves overflowing of a main river channel and a moving front traveling over previously dry areas.

The paper is organized as follows. In Section 2 we provide the model statement: both the 2D zoom model formulation (Section 2.1) and the 1D model formulation (Section 2.2). In Section 3 we describe the two-way information exchange between two models. In Section 4 we describe the waveform relaxation method and in Section 5 we introduce the joint assimilation-coupling algorithm. The numerical implementation is covered in Section 6: a description of the finite volume solver and the software DassFlow in Section 6.1, a description of the test configuration in Section 6.2 and of the adjoint code and minimization algorithm in Section 6.3. The numerical tests are covered in Section 7: the results of the WRM testing (Section 7.1) and the results of the JAC algorithm testing (Section 7.2). Then follow the Conclusion and the Appendix.

2 Problem statement

2.1 Two-dimensional zoom problem statement

For the general problem layout we refer to Fig.1. The 2D zoom problem is considered in the domain Ω_2 (zoom area) confined by the boundaries $\Gamma_{3,4,5,6}$ and the main channel (domain Ω_1) is confined by the boundaries $\Gamma_{1,2}$. We assume that the domains Ω_1 and Ω_2 are defined and they do not change in time. The moving wet/dry fronts are shown in Fig.1 in dashed lines. The bathymetry is given by the function $Z(x, y)$.

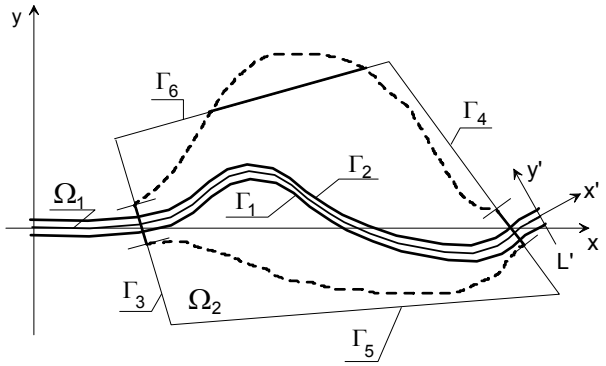

Fig. 1. General problem layout: the 1D main channel and the 2D zoom area

The equations describing the 2D shallow water flow are as follows:

$$U_t + A(U)_x + B(U)_y - S(U) = 0, \quad (x, y) \in \Omega_2(t), \quad t \in (0, T) \tag{1}$$

where

$$U = [\, h,\ q,\ p\,]^T$$

$$A(U) = \left[\, q,\ q^2/h + gh^2/2,\ qp/h \,\right]^T, \quad B(U) = \left[\, p,\ pq/h,\ p^2/h + gh^2/2 \,\right]^T$$

$$S(U) = [\, 0,\ gh(Z_x - f_x),\ gh(Z_y - f_y)\,]^T$$

Here $h = h(x, y, t)$ is the surface elevation, $q = q(x, y, t)$ and $p = p(x, y, t)$ are components of discharge, Z_x, f_x and Z_y, f_y are the bed slope and the friction slope associated to the x and y axes respectively, g is the gravity acceleration. The friction slope is defined by the Manning law via the coefficient $\mu = \mu(x, y)$ as follows:

$$f_x = \mu^2 (q^2 + p^2)^{1/2} q h^{-10/3}; \quad f_y = \mu^2 (q^2 + p^2)^{1/2} p h^{-10/3}$$

The initial condition is:

$$\forall (x,y) \in \Omega_2(0): \quad U(x,y,0) = U_0(x,y) \tag{2}$$

Later on we will always assume that the initial condition is known.

For each boundary Γ_l, $l = 3,4,5,6$ we define a rectilinear co-ordinate system (x'_l, y'_l) rotated anti-clockwise by the angle β_l in respect to the original co-ordinate system (x,y), such that the axis x'_l is pointed inward into Ω_2 in the direction which can be identified as a 'dominant characteristic direction' at Γ_l (see Fig. A.1(left) in the Appendix A). Let us note that this direction does not necessarily coincide with the inward normal to Γ_l. We write the boundary conditions for the open boundaries of Ω_2 in the characteristic form as follows

$$\begin{aligned} &(q'_l + (c - u'_l)h)|_{(x'_l,y'_l)\in\Gamma_l} = w_1|_{\Gamma_l} \\ &(p'_l - v'_l h)|_{(x'_l,y'_l)\in\Gamma_l} = w_3|_{\Gamma_l},\ \forall u' > 0 \end{aligned} \qquad l = 3,4,5,6 \tag{3}$$

The state vector $U'_l = [\,h,\ q'_l,\ p'_l\,]^T$ in the co-ordinate system (x'_l, y'_l) is related to the state vector U by the rotation $T(\beta_l)$ as follows

$$U'_l = T(\beta_l)U$$

where

$$T(\cdot) = \begin{pmatrix} 1 & 0 & 0 \\ 0 & cos(\cdot) & sin(\cdot) \\ 0 & -sin(\cdot) & cos(\cdot) \end{pmatrix} \tag{4}$$

In equations (3) $c = (gh)^{1/2}$, $u'_l = q'_l/h$, $v'_l = p'_l/h$ are linearized coefficients and the quantities $w_1|_{\Gamma_l} = w_1(x'_l, y'_l, t)|_{(x'_l,y'_l)\in\Gamma_l}$, and $w_3|_{\Gamma_l} = w_3(x'_l, y'_l, t)|_{(x'_l,y'_l)\in\Gamma_l}$ are the incoming characteristic variables of the 2D SWE to be imposed at the boundaries Γ_l. For details on the characteristic representation we refer to Appendix A. In (3) we assume that the flow at Γ_l always remains sub-critical. In the case when the bed and friction slopes are sufficiently mild the equations (1), (2), (3) should specify a well-posed 2D SWE problem. For details on numerical treatment of moving wet/dry fronts inside a fixed Ω_2 we refer to Section 6.1. From now on we always consider boundaries $\Gamma_{5,6}$ as the non-reflective open boundaries, i.e. we impose the following conditions

$$w_1|_{\Gamma_{5,6}} = 0, \quad w_3|_{\Gamma_{5,6}} = 0.$$

In many cases the boundaries of the main channel Γ_1, Γ_2 are naturally well contoured. From a mathematical point of view, the boundaries Γ_1, Γ_2 should be drawn to guarantee that the St-Venant formulation remains valid (the derivative of the wet cross-section area to the water elevation must exist and be continuous) and the effects of secondary (lateral) flows are not significant. In many practical situations the positions of Γ_3, Γ_4 along the median of the main channel can be satisfactorily estimated by considering topographic data. The boundaries Γ_5 and Γ_6 must be chosen far enough from the main channel. The availability of measured flow data outside the main channel could be another reason to use the zoom model in a certain area.

2.2 One-dimensional problem statement

The 1.5D model can be derived from the 2D SWE in two steps. First, the 2D SWE have to be considered in the curvilinear 'channel-following coordinates (x', y'), when x'-axis follows the median curve of the main channel and y' is the orthonormal to x'. The rotated equations consist of a principal part in the form (1), where state variables (h, q, p) are now replaced by $(h, q'p')$, and additional terms by order of magnitude $y'\partial\alpha/\partial x'$, where α is the angle between the x-axis and the tangent to the median curve of the main channel. These terms represent the curvature of the channel (see Appendix B for details). We consider the aggregate of those terms as a source term $\Psi^{curv}(x', y')$. The second step is to integrate rotated equations in y' from Γ_1 to Γ_2. Assuming that: a) $\partial u'/\partial y' = 0$; b) $\partial^2 h/\partial x'\partial y' = 0$, we get the Saint-Venant equations or, in the case when the main channel has a constant rectangular cross-section of width b, the 'dimensional 1D SWE as follows

$$\tilde{U}_t + \tilde{A}(\tilde{U})_{x'} - \tilde{S}(\tilde{U}) = \Psi, \quad (x') \in (0, L'), \quad t \in (0, T) \tag{5}$$

$$\tilde{U} = [\ H,\ Q\ ]^T\ ,\ \tilde{A}(\tilde{U}) = \left[\ Q,\ (Q)^2/H + g(H)^2/2\ \right]^T\ ,$$

$$\tilde{S}(\tilde{U}) = [\ 0,\ gh(Z_{x'} - f_{x'})]^T$$

where H is the wet cross-section area and Q is the total discharge. If H and Q are scaled by b, we get the classical 1D SWE variables. The initial condition for the 1D SWE problem is

$$\forall x' \in (0, L') : \quad \tilde{U}(x', 0) = \tilde{U}_0(x) \tag{6}$$

The characteristic analysis as presented in Appendix A, but applied to the 1D SWE problem (5) yields boundary conditions as follows

$$(Q + (\tilde{c} - \tilde{u})H)|_{x'=0} = W_1(x', t)|_{x'=0}, \quad (Q - (\tilde{c} + \tilde{u})H)|_{x'=L'} = W_1(x', t)|_{x'=L'} \tag{7}$$

where $\tilde{c} = (gH/b)^{1/2}, \tilde{u} = (Q/H)$ are linearized coefficients and the quantity $W_1(x', t)$ (incoming characteristic variable of the 1D SWE) is imposed. It is worth mentioning that the boundary conditions in the form (7) for the 1.5D model are not mandatory. For example, one can impose the inflow discharge, rating curves or elevation values, which are the classical BC used in river hydraulics.

The source term in equation (5) consists of two components:

$$\Psi = \Psi^{div} + \int_{\Gamma_1}^{\Gamma_2} \Psi^{curv} dy'; \quad \Psi^{div} = \left[p'_{\Gamma_1} - p'_{\Gamma_2}, \quad \left(\frac{q'p'}{h'}\right)_{\Gamma_1} - \left(\frac{q'p'}{h'}\right)_{\Gamma_2} \right]^T \tag{8}$$

The lateral boundary flux Ψ^{div} represents the overflow from the main channel (flow diversion). It models the storage area (static volume which may store water). The expression for Ψ^{div} is derived by empirical consideration. Another term Ψ^{curv} is the integrated curvature term, which is usually ignored in the 1.5D models. The formulation (5) is a standard 1.5D open channel flow model, which can be used as a single element of the network.

3 Information exchange principles

3.1 2D → 1D information transfer

To explain the information exchange between the 2D SWE and 1D SWE we turn directly to the finite-dimensional representation of problems given in (1) and (5). Let us consider a mesh consisting of finite volumes (cells) K_i, $i = 1, ..., N$, covering the 'zoom' area (Ω_2) in such a way that cell interfaces continuously reproduce boundaries of the main channel $\Gamma_{1,2}$ as shown in Fig.2. In the general case, the mesh need not necessarily be quadrangular. Assuming explicit time discretization, for the cell K_i

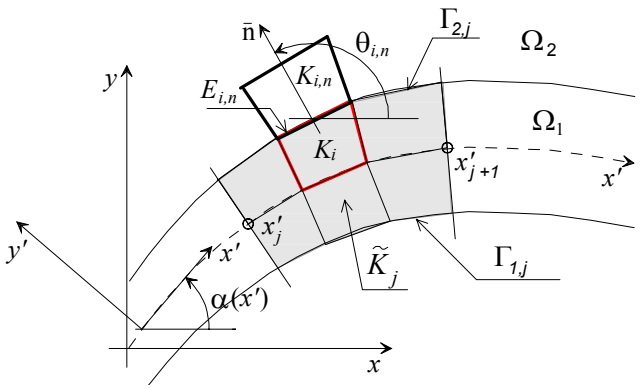

Fig. 2. Finite volume mesh

the model equation (1) can be approximated as follows

$$U_i^{m+1} = U_i^m - \tau \left(\frac{1}{|K_i|} \sum_{n=1}^{4} F_n(U_i) - S(U_i) \right)_{t=m\tau} \tag{9}$$

where $m = 0, ..., M$ is the time index, $\tau = T/(M+1)$ is the time step used for the 2D model integration, $F_n(U_i)$ are total fluxes of U via n^{th} edge $E_{i,n}$ of the cell K_i and $|K_i|$ is the cell surface. Let us denote $\delta t_m \in (m\tau,\ (m+1)\tau)$ the time interval between two successive time steps. We assume that any time dependent variable has a constant value for $t \in \delta t_m$, which is equal to its value at $t = m\tau$. For the edge we define a rotation $T(\theta)$ using (4), where θ is the angle between the normal $\vec{n}$ to the edge $E_{i,n}$ and the x-axis. Variables $V = [\ h,\ q_{\vec{n}},\ q_{\vec{\tau}}]$ are used to define a vector of local Godunov fluxes as follows

$$\Phi(V) = \left[q_{\vec{n}},\ q_{\vec{n}}^2/h + gh^2/2,\ q_{\vec{n}} q_{\vec{\tau}}/h \right]^T$$

Computing of $F_n(U_i)$ consists of three steps, see e.g. [19]:
a) compute the normal and tangent discharge components in the cell K_i and in its n^{th} neighbor $K_{i,n}$ adjacent to the edge $E_{i,n}$ (we refer to Fig.2) using the rotation as follows $V_i = T(\theta_{i,n})U_i$;
b)compute $\Phi(V)$ as an approximate solution of the local Riemann problem

$$\frac{\partial V}{\partial t} + \frac{\partial \Phi(V)}{\partial x_{\vec{n}}} = 0, \quad V(x,0) = \left\{ \begin{array}{c} V_i,\ \ x_{\vec{n}} < 0 \\ V_{i,n},\ x_{\vec{n}} > 0 \end{array} \right\}$$

c) compute fluxes of U_i using the inverse rotation $T^{-1}(\theta_{i,n})$, so we can eventually write

$$F_n(U_i) = T^{-1}(\theta_{i,n})\Phi(V) \tag{10}$$

For those cells belonging to Ω_1 the variables in the channel-following coordinates U', as well as fluxes $F_n(U_i')$ can be obtained using another rotation $T(\alpha)$ (refer to Fig.(2) for the definition of α) as follows

$$U' = T(\alpha)U, \quad F_n(U') = T(\alpha)F_n(U)$$

Let us assume that the domain $x' \in (0, L')$ is covered by a set of nodes $x_j',\ j = 1, ..., \tilde{N}$. We relate the 1D segment bounded by two nodes x_j' and x_{j+1}' and a 2D element of the main channel Ω_1 bounded by perpendiculars to x' constructed at these points (as we show in Fig.2). We denote this element (cell) $\tilde{K}_j$, its area $|\tilde{K}_j|$ and the arcs on the boundaries Γ_1, Γ_2 that belong to $\tilde{K}_j$ as $\Gamma_{1,j}, \Gamma_{2,j}$. Assuming explicit time

discretization, the equation (5) can be approximated in the finite-dimensional form as follows

$$\tilde{U}_j^{\tilde{m}+1} = \tilde{U}_j^{\tilde{m}} - \tilde{\tau}\left(\frac{1}{|\tilde{K}_j|}\sum_{n=1}^{2}\tilde{F}_n(\tilde{U}_j) - \tilde{S}(\tilde{U}_j) - \Psi_j\right)_{t=\tilde{m}\tilde{\tau}} \tag{11}$$

where $\tilde{m} = 0, ..., \tilde{M}$ is the time integration index, $\tilde{\tau} = T/(\tilde{M}+1)$ is the time step used for the 1D model integration, $\tilde{F}_n(\tilde{U}_j)$ are the fluxes of $\tilde{U}$ via the n^{th} edge of the cell $\tilde{K}_j$ (it can be defined by steps a)-c) as in the 2D case, when using $\theta_1 = 0$, $\theta_2 = \pi$). Similarly to the 2D, case we denote $\tilde{\delta}t_m \in (\tilde{m}\tilde{\tau},\ (\tilde{m}+1)\tilde{\tau})$ as the time interval between two successive time integration steps.

The first approach is to compute the overflow from the main channel as mass and momentum fluxes via the boundaries Γ_1 and Γ_2 using a current approximation of the 2D flow given by the zoom solution. Thus, we define piece-wise constant vector-functions $G_1(U')$, $G_2(U')$ as follows

$$G_1(U')|_{(x,y)\in E_{i,n},\, t=\delta t_m} = G_{i,n}^m(U')|_{\Gamma_1} := F_n(U_i')|_{t=m\tau},\ \ \forall(i,n):\ E_{i,n} \in \Gamma_1 \cap \Omega_2$$

$$G_2(U')|_{(x,y)\in E_{i,n},\, t=\delta t_m} = G_{i,n}^m(U')|_{\Gamma_2} := F_n(U_i')|_{t=m\tau},\ \ \forall(i,n):\ E_{i,n} \in \Gamma_2 \cap \Omega_2$$

Since the 1D state consists of the components (H', Q'), we need to retain only the first two of three components of G. This can be achieved by multiplying G from the left by a diagonal matrix $I_0 = diag[1, 1, 0]$. Thus, the overflowing in the 1D model can be compensated using the source term $\Psi = \{\Psi_j^{\tilde{m}}\}$ as follows

$$\Psi_j^{\tilde{m}} = \frac{1}{\tilde{\tau}|\tilde{K}_j|}\int_{\tilde{\delta}t_m} dt\ \ (\int_{\Gamma_{2,j}} I_0\, G_1 d\Gamma - \int_{\Gamma_{1,j}} I_0\, G_2 d\Gamma) \tag{12}$$

A more accurate approach is based on a defect correction term that originates from the multi-grid method, see e.g. [4]. If A_f and A_c are spatial operators defined on a fine and a coarse grid respectively, U is a state variable and R is a fine-to-coarse projection (restriction) operator, then the defect correction term used in the coarse grid problem approximation reads as follows

$$d = RA_f(U) - A_c(RU)$$

Let us define a piece-wise constant vector-functions $G(U)$ and $\tilde{G}(\tilde{U})$ such that

$$G(U)|_{(x,y)\in K_i,\, t\in\delta t_m} = G_i^m(U) := \frac{1}{|K_i|}\sum_{n=1}^{4} F_n(U_i) - S(U_i);\ \ \forall i : K_i \in \Omega_2 \cap \Omega_1$$

$$\tilde{G}(\tilde{U})|_{x'\in\tilde{K}_j,\, t\in\tilde{\delta}t_m} = \tilde{G}_j^{\tilde{m}}(\tilde{U}) := \frac{1}{|\tilde{K}_j|}\sum_{n=1}^{2} \tilde{F}_n(\tilde{U}_j) - \tilde{S}(\tilde{U}_j);\ \ \forall j :\ \tilde{K}_j \in \Omega_1 \cap \Omega_2$$

Here $G(U)$ is the action of the finite-dimensional 2D SWE spatial operator on a state vector U as in (9) and $\tilde{G}(\tilde{U})$ is the action of the 1D SWE spatial operator on a state vector $\tilde{U}$ as in (11). We also introduce a projection (restriction) operator R that computes average values over $\tilde{K}_i$ and $\tilde{\tau}$

$$R_j^{\tilde{m}}\varphi = \frac{1}{\tilde{\tau}|\tilde{K}_j|}\int\limits_{\tilde{\delta}t_m}\int\limits_{\tilde{K}_j}\varphi\, d\Omega_1 dt$$

Eventually, the source term $\Psi = \{\Psi_j^{\tilde{m}}\}$ for the 1D model can be defined as follows

$$\Psi_j^{\tilde{m}} = R_j^{\tilde{m}}\, I_0 G(U') - \tilde{G}_j^{\tilde{m}}(R_j^{\tilde{m}}\, I_0 U') \tag{13}$$

Let us note that for matching uniform grids, without curvature and friction, the values Ψ obtained by (12) and (13) are equivalent. Otherwise, the overflowing fluxes still remain a major contribution to Ψ, because in integration over $\tilde{K}_j$ interior fluxes between edges of the 2D cells cancel out. Obviously, the defect correction term as specified in (13) is a generalization of the classical multi-grid defect correction, since it takes into account the dimensional heterogeneity.

This approach is more accurate when both the spatial discretization in Ω_1 and time integration step for the 2D model are finer than those used for the 1D model. This is the case in practical applications. Otherwise, one must use the 'overflow' formula (12). Let us also note that the 1.5D SWE solver in the existing open-channel network model can be implemented using any discretization scheme. The scheme (11) is used to derive (13) only.

3.2 1D → 2D information transfer

For coupling the 1D and 'zoom' models at the boundaries $\Gamma_{3,4}$ we use a characteristic approach. We assume that the dominant incidence direction at Γ_3 coincides with the tangent to the median curve of the main channel. At Γ_4 the dominant incidence direction is opposite to it. Let us denote

$$\delta W_1(t)|_{\Gamma_l} := \int\limits_{\Gamma_l} w_1(x_l', y_l', t)\, d\Gamma - W_1(x', t)|_{\,x'\in\Gamma_l}, \quad l = 3, 4 \tag{14}$$

where w_1 is defined in (3) and W_1 in (7). Actually we demand that the incoming characteristic quantities across the coupling interfaces are continuous. This condition can be written as follows

$$\delta W_1(t)|_{\Gamma_l} = 0, \quad l = 3, 4, \;\; t \in (0, T) \tag{15}$$

Let us note that equations (14)-(15) do not specify $w_1|_{\Gamma_l}$ uniquely. That is, the distribution of $w_1|_{\Gamma_l}$ along Γ_l remains unknown. The component $w_3|_{\Gamma_l}$, $l = 3, 4$ in (3) simply has no equivalent quantity in the 1D formulation.

In order to write down condition (15) in the finite-dimensional form we assume that after discretization w and W are piece-wise constant functions such that

$$w_1|_{(x,\, y)\in K_i,\ t\in\delta t_m} = (w_1)_i^m;\ \ i = 1, ..., N,\ m = 0, ..., M$$

$$W_1|_{x'\in\tilde{K}_j,\ t\in\delta\tilde{t}_m} = (W_1)_j^{\tilde{m}};\ \ j = 1, ..., \tilde{N},\ \tilde{m} = 0, ..., \tilde{M}$$

Therefore, the definition for $\delta W_1|_{\Gamma_l}$ becomes as follows

$$\delta W_1^m|_{\Gamma_l} = \int\limits_{\Gamma_l} (w_1)_i^m|_{\forall K_i\cap\Gamma_l\neq 0}\, d\Gamma - I(i,m)W_1, \quad l = 3, 4$$

where $I(i, m)$ is a prolongation operator which interpolates the piece-wise constant function W defined on a coarse spatial-temporal mesh to a space-time cell $(K_i, \delta t_m)$ defined by parameters i and m ($I(i, m)$ is just a formal notation for an interpolation algorithm). In numerical tests we use local cubic splines to interpolate W in space and linear interpolation in time.

4 Waveform relaxation (global time Schwarz) coupling method

Let us assume that we know the initial conditions $U(\Omega_2, 0)$ and $\tilde{U}(\Omega_1, 0)$, and the boundary conditions for the 1D problem $W_1(0, t)$, $W_1(L', t)$. In order to define boundary conditions at boundaries $\Gamma_{3,4}$ we have to specify functions $w_1|_{\Gamma_{3,4}}$, $w_3|_{\Gamma_{3,4}}$. However, the equations (14)-(15) define a single integral constraint on $w_1|_{\Gamma_{3,4}}$, which can be satisfied by an infinite number of functions. One could assume a-priori that $w_1|_{\Gamma_{3,4}}$ are distributed uniformly along $\Gamma_{3,4}$, (or are proportional to $h^{3/2}$) and $w_3|_{\Gamma_{3,4}} = 0$. These are the most straightforward assumptions, which could be justified only if the 2D flow at the boundaries $\Gamma_{3,4}$ of the 'zoom' area exhibits essentially 1D behavior. We shall call a model whose solution $\{U, \tilde{U}\}$ satisfies simultaneously (1)-(3), (5)-(7), (13) and (15) a 'coupled model'. We seek an approximate solution of this model using the WFR by taking the following steps:

a) Set $\Psi_j^{\tilde{m}} = 0$, $\forall\tilde{K}_j \in (\Omega_1 \cap \Omega_2)$;
b) given the initial condition (6), boundary conditions $W_1(0, t)$, $W_1(L', t)$ and the source term $\Psi_j^{\tilde{m}}$ solve the 1D problem (5) for $x' \in (0, L')$, $t \in (0, T)$;
c) compute boundary conditions for the 'zoom' model $w_1|_{\Gamma_{3,4}}$, to satisfy exactly condition (15) using a certain distribution rule and a-priori specified $w_3|_{\Gamma_{3,4}}$;
d) given the initial condition (2), boundary conditions $w_1|_{\Gamma_{3,4}}$ and $w_3|_{\Gamma_{3,4}} = 0$, solve

the 'zoom' problem for $(x, y) \in \Omega_2(t)$, $t \in (0, T)$;
e) compute source terms to the 1D model $\Psi_j^{\tilde{m}}$, $\forall \tilde{K}_j \in (\Omega_1 \cap \Omega_2)$ given the current approximation of the 'zoom' solution using (12) or (13);
f) check the stopping criterion

$$\sum_{\tilde{m}=0}^{T/\tilde{\tau}} \sum_{j=1}^{\tilde{N}} \left((\Psi_j^m)^{k+1} - (\Psi_j^m)^k \right)^2 > \epsilon_1$$

where ϵ_1 is a small positive number, k is the iteration number.
g) if satisfied, return to b), stop iterating otherwise.

The WFR algorithm can be used to superpose a 'zoom' model over any chosen part of an open-channel network model. Even though we consider a simple configuration here (a single segment of the network) the approach is general. For example, one could improve the representation of a complex junction by superposing a 'zoom' model.

5 Joint assimilation-coupling algorithm (JAC)

In Section 4 we have introduced the coupling of the two models using the WFR method. For this method a-priori assumptions are necessary. That is, we must choose a-priori a particular shape for functions $w_1|_{\Gamma_{3,4}}$ (i.e. to distribute the 1D information along the 2D boundary) and specify $w_3|_{\Gamma_{3,4}}$. Let us also recall that in practice, the global 1.5D model is solved on a much coarser mesh with typical ratios of $10^1 - 10^2$ for the space mesh size and $10^2 - 10^3$ for the time step. In order to overcome possible difficulties related to the inconsistency of models a coupling method based on an optimal control approach can be used.

To apply this method we consider (15) in a weak form as follows:

$$J_c = J_1 + J_2, \quad J_1 = \int_0^T (\delta W_1(t)|_{\Gamma_3})^2 dt, \quad J_2 = \int_0^T (\delta W_1(t)|_{\Gamma_4})^2 dt \tag{16}$$

Now, instead of solving the strongly coupled model as previously, we formulate the coupling problem as an optimal control problem:
find the minimum of the cost functional

$$J(w_1(t)|_{\Gamma_{3,4}}, w_3(t)|_{\Gamma_{3,4}}) = J_c + J_a \tag{17}$$

subjected to constraints (1)-(3), (13), (5)-(7).

We shall call the set of constraints (1)-(3), (13), (5)-(7) a 'one-way relaxed model'. Indeed, as compared to the 'coupled model' this model does not include condition (15), which demands the characteristic variables at the models' interfaces to be continuous. This condition is weakly imposed using optimal control. The term J_a stands for penalty terms, which may include the same a-priori assumptions used in the WFR algorithm, but written in a weak integral from.

The drawback of the optimal control based coupling method could be its computational cost because it needs the control loop iterations. This might be an obstacle to the use of this method. However, the situation becomes different if the problem is considered in the context of DA, which needs the control loop iterations anyway.

Let us denote $K_{i(n)},\ n = 1, ..., \hat{N}$ a subset of cells where the measurements of certain components of the state vector U are available. Here $\hat{N}$ is a number of such cells, $i(n)$ is a global index of a cell from the full set of cells $K_i,\ n = 1, N$. We denote data measured in $K_{i(n)}$ as $\hat{U}_{i(n)}$. In order to select certain components from $\hat{U}_{i(n)}$ we introduce an observation operator C_n that is simply a vector of weights equal to 0 or 1. A classical DA cost functional is

$$\hat{J} = \sum_{n=1}^{\hat{N}} \int_0^T C_n (U_{i(n)} - \hat{U}_{i(n)})^2 \ dt \tag{18}$$

where $\hat{J}$ depends on the unknown controls.
Let us assume, for example, that the BC at the ends of the 1.5D segment $W_1(0,t)$, $W_1(L',t)$ are sought. Then the optimal control problem which solves the coupling and DA problems simultaneously is:
find the minimum of the generalized cost functional

$$J(W_1(0,t), W_1(L',t), w_1(t)|_{\Gamma_{3,4}}, w_3(t)|_{\Gamma_{3,4}}) = J_c + \rho \hat{J} \tag{19}$$

subjected to constraints (1)-(3), (13), (5)-(7).

All functions $W_1(0,t)$, $W_1(L',t)$, $w_1(t)|_{\Gamma_{3,4}}$, $w_3(t)|_{\Gamma_{3,4}}$ are considered here as unknown controls. One can see that the generalized cost functional J consists of the term J_c, which represent the coupling problem, and the term $\rho\hat{J}$, where ρ is a weight factor, which represents the DA problem. Let us note that the term J_a could be also retained, if necessary, although its presence is no longer mandatory.

A gradient-type optimization algorithm is used to solve the minimization problem for (19) under constraints (1)-(3), (13), (5)-(7). The gradient is computed by solving the adjoint of the one-way relaxed model.

6 Numerical implementation

6.1 Finite volume solver and DassFlow software

All schemes and algorithms presented in the paper are implemented in the software called DassFlow, [9]. The 2D SWE (1)-(3) are solved numerically using a finite-volume method. Here, to simplify the implementation, the mesh is structured rectangular with mesh-sizes (h_x, h_y). Time discretization is done using the Euler explicit scheme, hence the CFL stability condition must be satisfied. Space discretization is based on rotation of the 2D SWE equations for each edge of the computational cell. Thus we reduce the 2D SWE to a set of the 1D local Riemann problems, see e.g. [19], [9]. Fluxes are computed using the HLLC solver, see [19]. This first-order scheme handles correctly the transition between sub-critical and super-critical flows, unlike most other first-order schemes. This is important for reliable front propagation modeling. The bed slope is included into the source term of the 1D local Riemann problems as described in [20]. The treatment of the friction term is explicit in time. The treatment of dry/wet fronts is done as described in [19], p.197. We introduce a threshold $h_\epsilon > 0$. If the water elevation h in a given computational cell is less than h_ϵ, then the cell is considered dry and the velocity components there are put to zero. A typical value of the threshold chosen in computations is $10^{-2} - 10^{-3}m$. We refer to [9] for more details and benchmark results obtained using the present solver.
The 1D model is discretized on a uniform spatial mesh with a mesh-size $\tilde{h}_x$ and solved similarly: we use the same 1D HLLC Riemann solver. The friction term and the source term Ψ are discretized explicitly in time.
The implementation of the characteristic BC is done as follows, see e.g. [10]. We compute the state variables in 'ghost' cells $K_{i,n}$ adjacent and symmetric to the boundary cells K_i over the edge $E_{i,n} \in \Gamma_l$ using the inverse rotation

$$U = T^{-1}(\beta_l)U'_l$$

where $U'_l = [h,\ q'_l,\ p'_l]^T$ are computed as follows

$$h = \frac{1}{2}\left(\frac{w_1|_{\Gamma_l}}{c} - \frac{w_2|_{\Gamma_l}}{c}\right)$$

$$q'_l = \frac{1}{2}\left(\left(1 + \frac{u'_l}{c}\right) w_1|_{\Gamma_l} + \left(1 - \frac{u'_l}{c}\right) w_2|_{\Gamma_l}\right)$$

$$p'_l = w_3|_{\Gamma_l} + v'_l h,\ \ \forall u' > 0$$

Above $c = (gh_l^{1/2})_{t-\tau}$, $u'_l = (q'_l/h)|_{t-\tau}$, $v'_l = (p'_l/h)_{t-\tau}$ are linearized coefficients, $w_1(\Gamma_l, t)$ and $w_3(\Gamma_l, t)$ are incoming characteristic variables (3) to be imposed, w_2 is

the outgoing characteristic variable defined as follows

$$w_2(\Gamma_l, t) = (q'_l - (c + u'_l)h)|_{(x,y)\in\Gamma_l}$$

This quantity must be extrapolated to the center of the cell $K_{i,n}$ from the interior in the direction opposite to the dominant incidence direction defined by the angle β_l. For extrapolation we use a local cubic spline representation of w_2.

6.2 Domain configuration and reference flow

For all numerical tests we use a simplified problem layout as shown in Fig.3(left). The bathymetry is defined as a uniform bed with a slope in the x-direction equal to 0.2% as shown in Fig.3(right). Thus, the river flows from the left to the right. The main channel width $b = 40m$, the relative height of the high bank of the main channel measured from the uniform bed level $dZ_{high} = 6m$ and the height of the low bank $dZ_{low} = 2m$. The boundary at $y = 0$ is a no-flow boundary, i.e. a wall. For simplicity, boundaries of the zoom area Γ_3, Γ_4 are chosen beyond the area where the overflowing may happen. Despite the simplifications this idealized scheme allows the basic ideas of the proposed approach to be verified. The Manning coefficient is uniform and $\mu = 0.04$, the threshold $h_\epsilon = 10^{-2}m$.

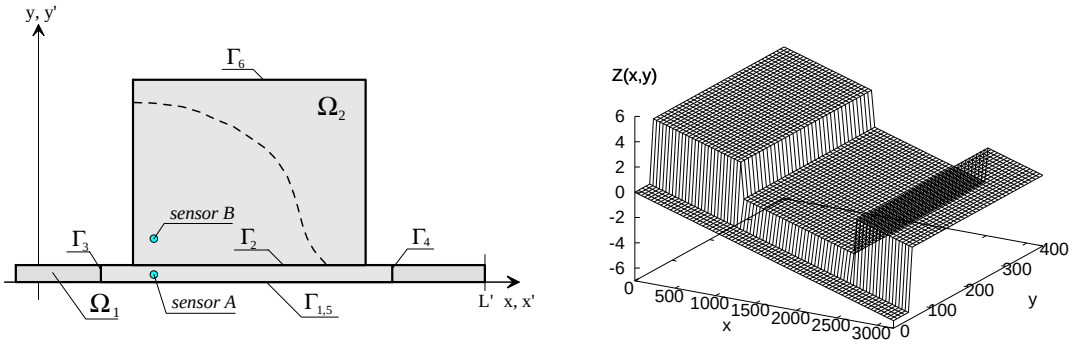

Fig. 3. Simplified problem layout and bathymetry used in numerical tests

To enable analysis of results we compute a reference flow pattern by solving the 2D SWE problem in the entire spatial domain $\Omega_0 = \Omega_1 \cup \Omega_2$. Beforehand, we solve the 2D problem for $t \in (0, T^*)$ starting from an arbitrary unphysical initial condition $h(\Omega_1, 0) < dZ_{low}$, $h(\Omega_0 \notin \Omega_1, 0) = 0$, $q(\Omega_0, 0) = 0$, $p(\Omega_0, 0) = 0$ applying a constant value of the upstream boundary control $w_1(0, y, t) = w^*$ and keeping the open non-reflective boundary downstream ($w_1(L, y, t) = 0$). The time interval is chosen to obtain an almost steady state solution at $t = T^*$, i.e. such that the state variables do not change on time significantly. Also, we choose a value w^* such that $h(\Omega_1, T^*)$ is very close, but smaller than dZ_{low}, i.e. the flow is on the brink of flooding. This solution can be used as a meaningful initial condition for further computations.

We compute it once (for the chosen set of parameters, bathymetry configuration, etc.) and keep it in memory. Thus, we start the main computations for $t \in (0, T)$ using computed $U(\Omega_0, T^*)$ as the initial condition. We add a time-dependent positive component to w^*, which creates a surge wave propagating downstream. When the wave reaches the low bank it starts overflowing and produces a wetting front traveling over the previously dry area. This process is illustrated in Fig.4, where the surface elevation of the flow in Ω_2 for different times is presented. The boundary condition that generates the reference solution is as follows

$$w_1(0, y, t)b = w^* + 1.2(1 - cos(\pi t/480)10^4,\ m^2/s,\ \ w^* = 0.5 \times 10^4\ m^2/s$$

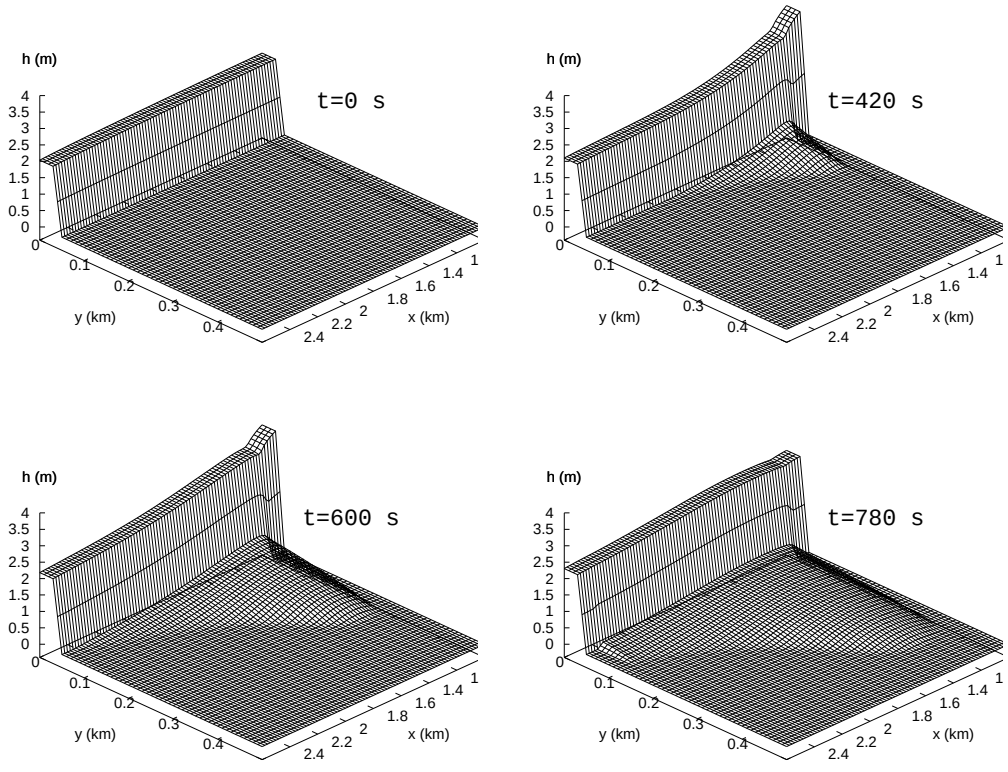

Fig. 4. Reference flow (surface elevation h) for different times

In all numerical examples we solve the reference problem and the zoom problem using the same spatial and time discretization. We refer to a consistent discretization when the 1D model solution is obtained with the same spatial mesh-size $\tilde{h}_x = h_x$ and time step $\tilde{\tau} = \tau$ as the 2D problem, and to an inconsistent discretization otherwise.

6.3 Adjoint code and minimization process

When using the JAC procedure, one must minimize the cost functional (19). This is done using a descent algorithm, thus one must compute the gradient of J. We compute it classically by introducing the adjoint of the one-way relaxed model. In DassFlow, [9], this is done by differentiating directly the forward code which solves the forward model equations (1)-(3), (13), (5)-(7) (as enumerated) and computes (19) afterwords. We use the Automatic Differentiation (AD) engine TAPENADE developed at INRIA, TROPICS [13]. The adjoint code, produced in this way, is verified using classical tests. The minimization algorithm is the L-BFGS algorithm (routine M1QB3, see [12]). We refer to [9] for more details.

7 Numerical results

7.1 Waveform relaxation coupling procedure

In this section we suppose that the BC of the 1D model are given. We couple the two models using the WFR algorithm (described in Section 4). Of course, no data assimilation is planned at this stage.

Coupling with consistent meshes. We compute solutions using a consistent discretization, such that $\tilde{\tau} = \tau = 0.1\,s$, $\tilde{h}_x = h_x = 20$. In Fig.5(left), the reference solution in Ω_1 at time $t = 600s$ is presented by a faint solid line, while the 1D coupled solutions after k iterations of the WFR algorithm are presented by bold lines. One can see that without the correction term ($k = 0,\ \Psi = 0$) the 1D coupled solution deviates significantly from the reference solution in Ω_1, but after just two or three iterations follows it very closely. The convergence rate expressed in terms of the norm J_c ((16), computed after step b) of the WFR algorithm, i.e. before (15) is satisfied exactly), is about two orders of magnitude per iteration, until it reaches a consistency threshold. This is usually a very small value in the case of consistent discretization. Thus, in practice we approach the optimal convergence rate of the WFR method, which must converge in two iterations, see [8]. In Fig.5 (right) we show the reference solution in the whole domain (in faint solid lines) and the zoom solution in the zoom area Ω_2 (in bold lines). Every line here corresponds to the flow slice made at $y = (j - 1/2)h_y,\ j = 1, ..., 12$. One can see a nearly perfect agreement between the reference and zoom solutions. The same presentation style is used throughout Section 7.

Let us point out that the main channel in the 2D model discretization can be represented correctly by using only one cell in width (i.e. $b/h_y = 1$). We performed numer-

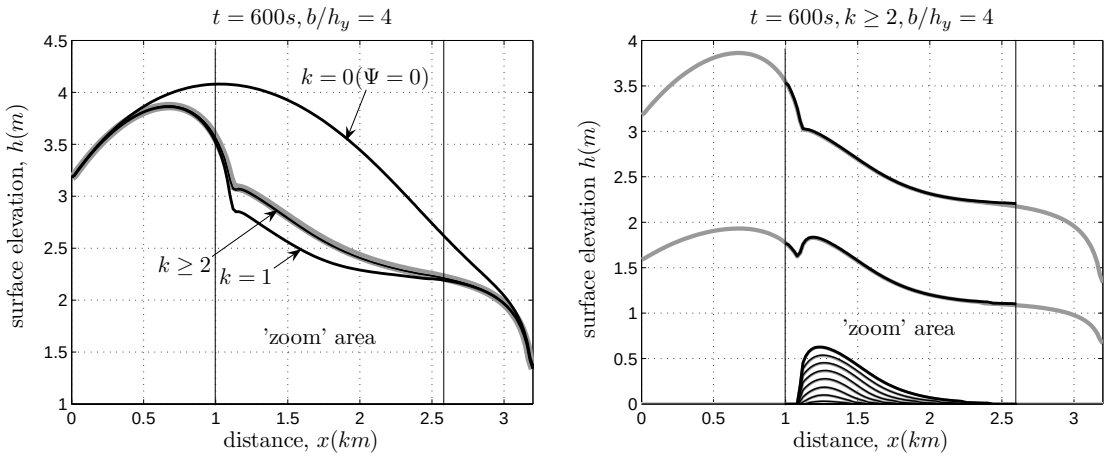

Fig. 5. WFR method, consistent discretization. Left: The 1.5D solution in the main channel. Right: reference solution and the 2D zoom solution.

ical tests which showed that if the main channel is discretized using two ($b/h_y = 2$) and four ($b/h_y = 4$) cells in width this improves the accuracy. This improvement, however, is not very significant. Thus, in all numerical examples that follow we use $h_y = b = 40m$.
In Fig.5 (right) we show the reference solution in the whole domain (in faint solid lines) and the zoom solution in the zoom area Ω_2 (in bold lines). Every line here corresponds to the flow slice made at $y = (j - 1/2)h_y,\ j = 1, ..., 20$. One can see a nearly perfect agreement between the reference and zoom solutions. The same presentation style is used throughout Section 7.
Results presented in Fig.5 could be equally obtained either by computing the overflow (12) or the defect correction (13), since for a consistent discretization (and without curvature and friction) both expressions (12) and (13) produce nearly the same value of Ψ. However, this is not the case if we use an inconsistent discretization.

Coupling with inconsistent meshes. In practice, the 1D model is solved on a much coarser spatial mesh and with a much larger time step than the 2D model. For further modeling we keep the following ratios: $\tilde{\tau}/\tau = 10^2$, $\tilde{h}_x/h_x = 10^1$ and, as before, we use $\tau = 0.1\,s$, $h_x = 20\,m$, $h_y = 40\,m$.
First, we compute the 1D coupled and zoom solutions using the overflow formula (12). The results at $t = 600\,s$ are presented in Fig.6, the elevation h to the left and the velocity u to the right.

In Fig.6(left/right), we show the reference solution (in faint solid lines), the zoom solution in Ω_2 (in bold solid lines) and the 1D coupled solution (solid line with markers). One can see that both the 1D coupled and zoom solutions differ from the reference value: in particular the 1D coupled solution deviates from the reference solution in Ω_1, apparently showing the presence of a cumulative error. The zoom solution deviates mostly near the boundaries of the zoom area, since the BC of the zoom model are tied to the 1D solution at interface.

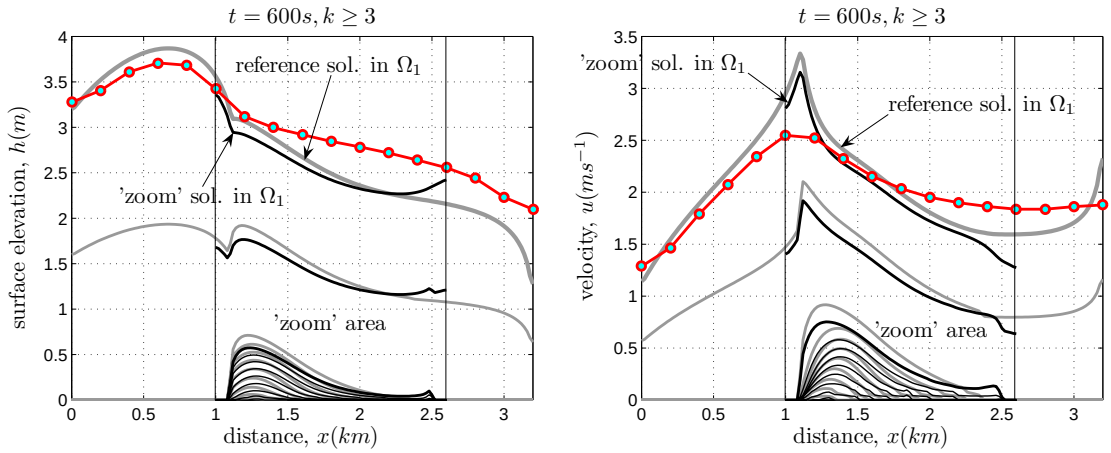

Fig. 6. WFR method, inconsistent discretization, using overflowing (12)

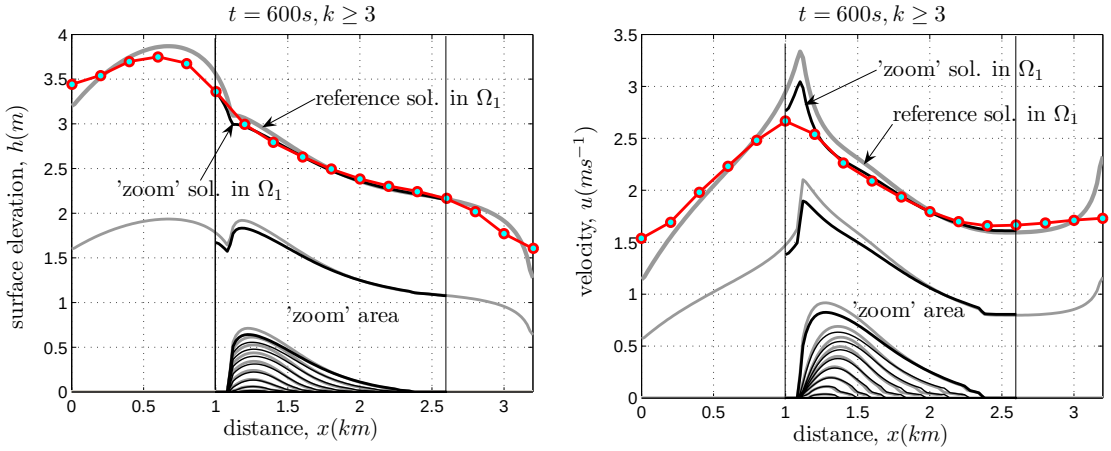

Fig. 7. WFR method, inconsistent discretization, using defect correction (13)

Next we compute the 1D and zoom solutions using the defect correction formula (13). The results at time $t = 600\,s$ are presented in Fig.7. Here we use the same presentation style as in Fig.6. One can see that the 1D coupled solution approximates the reference solution in Ω_1 much more closely than before. The zoom solution is also better, particularly near the downstream boundary of Ω_2. This last result shows that the defect correction term improves the coupled solution (both in the main channel and in the zoom area) when the two models are discretized with inconsistent spatial-temporal meshes.

7.2 Joint assimilation - coupling (JAC) procedure

In the JAC procedure, we compute the gradient of (19) with respect to all controls $W_1(0,t)$, $W_2(L',t)$, $w_1(t)|_{\Gamma_3}$, $w_2(t)_{\Gamma_4}$, $w_3(t)|_{\Gamma_{3,4}}$ by computing the adjoint as described

previously.
The unknowns of the 2D model are the incoming characteristic variables $w_1(t)|_{\Gamma_{3,4}}$ ($w_3(t)|_{\Gamma_{3,4}} = 0$), while for the 1D model we seek to identify the upstream incoming characteristic variable $W_1(0,t)$, assuming a non-reflective open boundary downstream i.e. $W_1(L',t) = 0$.
Measurements (water elevation and the components of discharge) are collected at two points located within the zoom area as shown in Fig.3(left), every $\nu_{obs} = 6\ s$. The exact location of the sensors is as follows: $x_1 = 290\,m$, $y_1 = 20\,m$ for sensor A, $x_1 = 290\,m, y_2 = 140\,m$ for sensor B. We conduct identical twin experiments; this means that given the controls, we generate synthetic data by solving the 2D reference problem, then we seek to identify those controls by assimilating the same synthetic data.
In the assimilation examples presented in Fig.8 and Fig.9, we use a consistent dis-

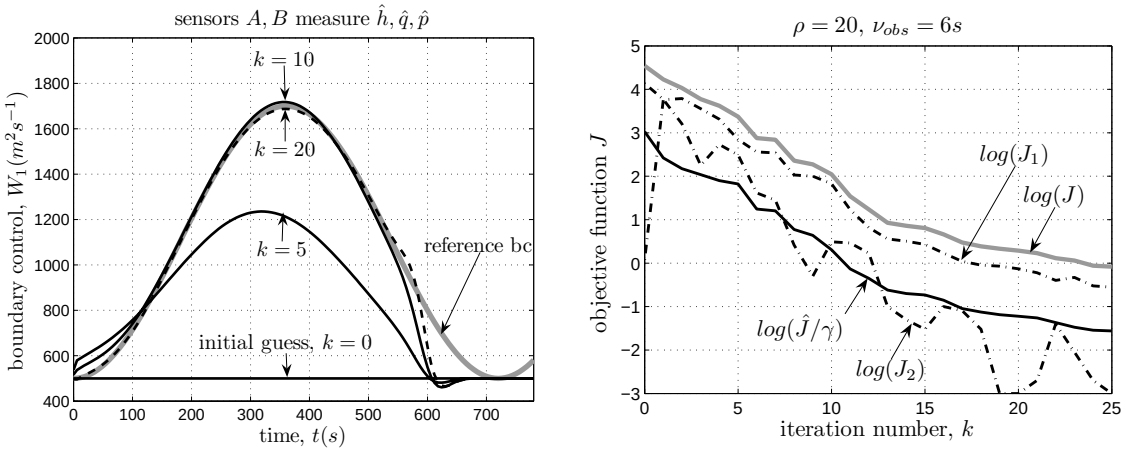

Fig. 8. Assimilation of data ($\hat{h}$, $\hat{q}$, $\hat{p}$) by JAC algorithm: inflow BC $W_1(t)$ after k iterations (left); the convergence history in *log*-scale (right). Consistent discretization.

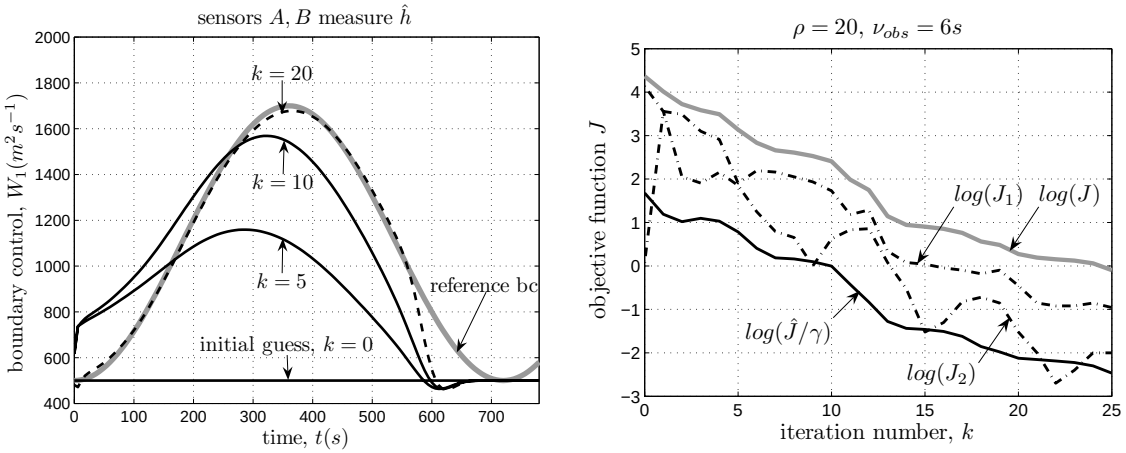

Fig. 9. Assimilation of data ($\hat{h}$) by the JAC algorithm: inflow BC $W_1(t)$ after k iterations (left); the convergence history in *log*-scale (right). Consistent discretization.

cretization. In Fig.8(left) and Fig.9(left), we present the reference BC (in faint solid lines) and its retrieved value after k iterations of the JAC algorithm (in bold solid lines). The final solution (corresponds to the largest k) is presented by dashed lines. A line that corresponds to $k = 0$ is the initial guess. To the right, we present the convergence history for J and for its components $\hat{J}$, J_1, J_2. These examples show that the JAC procedure converges: this allows the unknown BC of the 1.5D model to be identified (by assimilating data collected both in the main channel and the zoom area) and both models to be accurately coupled at same time.
When both measurements of discharge $\hat{q}$, $\hat{p}$ and elevation $\hat{h}$ are assimilated (Fig.8) we need about 10 iterations to get a reasonable estimation of the reference value and about 20 iterations to get very close. Let us point out that there exists a blind period in the vicinity of $t = T$, where the inflow BC cannot be identified.
In Fig.9, we present the same case, but measurements of elevation $\hat{h}$ only are assimilated. In this case, one needs more iterations to get a good estimation of the inflow BC, although the convergence rate is nearly the same. Again, this shows that the JAC procedure allows us to identify the unknown inflow BC of the 1D model and to couple accurately both models simultaneously by assimilating elevation data only.

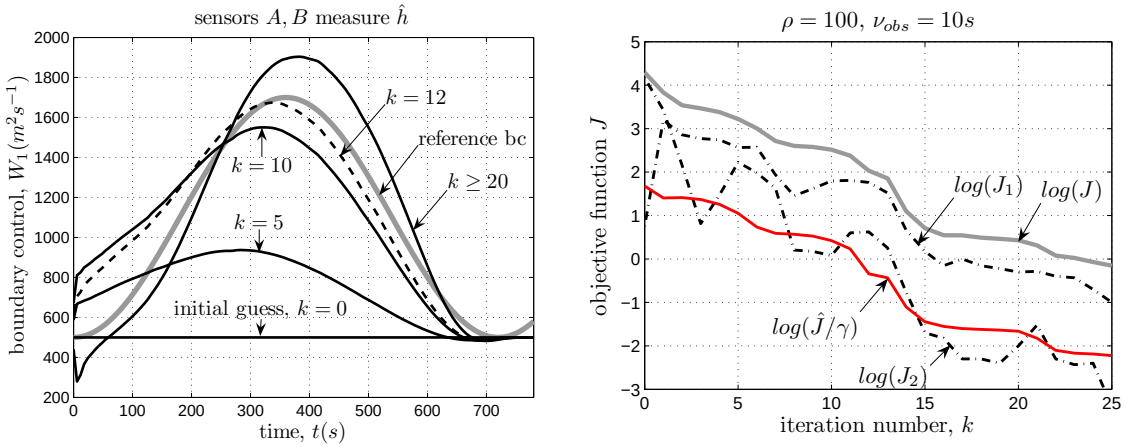

Fig. 10. Assimilation of data (h) by the JAC algorithm: $W_1(t)$ after k iterations (left); the convergence history, *log*-scale (right). Inconsistent discretization.

In the next assimilation example, we use an inconsistent discretization. That is, the 1D model is solved on a much coarser spatial-temporal mesh than the reference and zoom models. Ratios between spatial mesh-sizes and time steps are the following: $\tilde{\tau}/\tau = 10^2$, $\tilde{h}_x/h_x = 10^1$. Only measurements of elevation h are used.
In Fig.10(left) we show the reference BC (in faint solid line) and its retrieved estimation after k iterations (in bold solid lines). In Fig.10(right) we show the convergence history. One can see that the convergence rate is the same as in the two previous examples (consistent discretization), but the estimation finally deviates from the reference value.
There exists an iteration number $k_{opt} \approx 12$ (in dashed line) when we can observe the best match between the estimate and the reference value. If we continue to iterate the estimates deviate approaching the value shown at $k = 20$. This is a standard

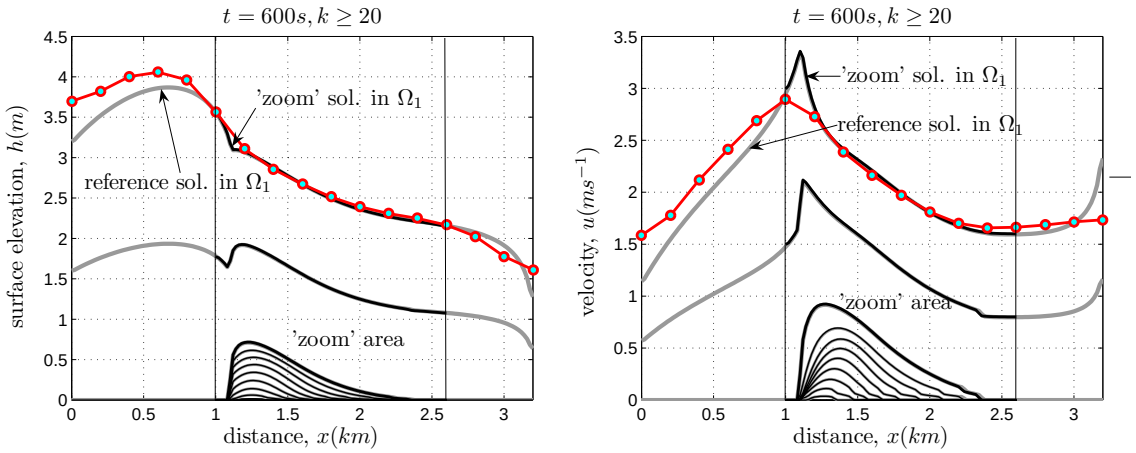

Fig. 11. Flow example after DA. Corresponds to Fig.10

behavior that the solution of an inverse problem could exhibit in the presence of errors. In our case this is a model error. Indeed, the synthetic measurements are generated by the 2D reference model discretized on a fine spatial-temporal mesh, while we assimilate data into the 1D model discretized on a coarse spatial-temporal mesh (even though this is done via the zoom model). Let us note that the control problem for the generalized cost functional (19) is actually solved. The value of J is reduced by factor 10^4, the 1D flow within the main channel inside the zoom area is a nearly perfect (as good as the spatial discretization allows) match with the reference flow pattern, as can be seen in Fig.11. This result, however, is achieved by a value of control $W_1(0,t)$ which does not match the reference value. This shows that the exact solution of the control problem for (19) is not necessarily the best estimation of the sought control function. In fact, this difficulty is shared by most inverse problems, see e.g. [1]. We refer to Appendix C for details. One approach to deal with this difficulty is to stop iterations guided by the generalized residual rule [18].

It is worth noting that in the latest example (inconsistent discretization, Fig.11), the 1D flow reproduces well the reference flow inside the zoom area, but deviates from the reference value outside the zoom area. This behavior can be observed for any time instant $t \in (0,T)$. This is because the solution of the 1D model is close to the 2D zoom solution in that area since both are coupled and the zoom model is solved on a fine mesh.

In the last numerical test we assimilate data available in the zoom area outside the main channel, which cannot be assimilated using the 1.5D model. The data is collected by sensor B, Fig.3(left), which is located at a distance $y = 100\,m$ from the overflow boundary Γ_2. We use a special form of the reference BC $W_1(0,t)$ as shown in Fig.12(left) by a faint solid line. Up to $t \approx 300\,s$ the value $W_1(0,t)$ is less than a 'no-overflow' level $w^* = 500 m^2 s^{-1}$. This is done to increase the period when this sensor remains in a dry area. The readings of the sensor B are shown in Fig.12(left)

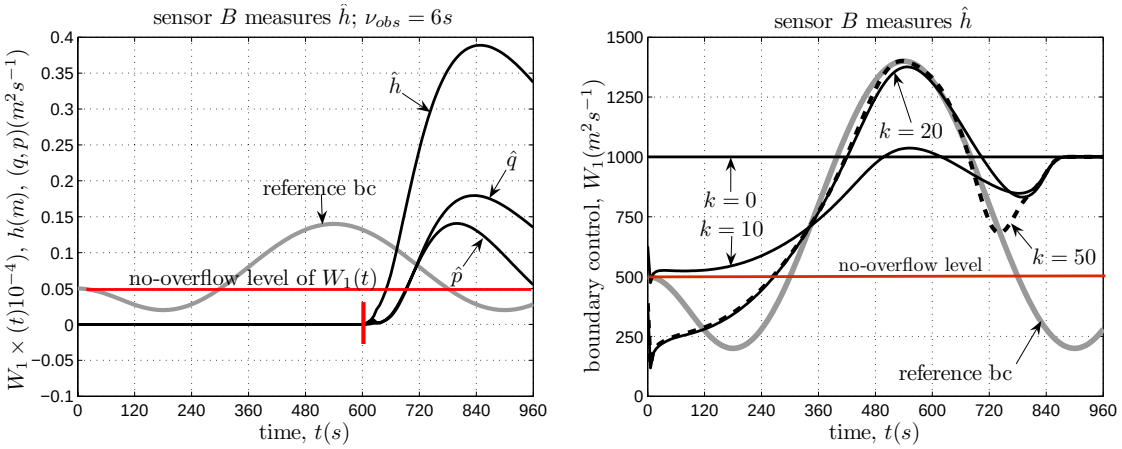

Fig. 12. Reference BC and readings by the dry field sensor B (left). Assimilation of data (h) by the JAC algorithm: $W_1(t)$ after k iterations (right).

by bold solid lines. We note that up to $t \approx 600\,s$ no flow information is recorded. For this test case we use a consistent discretization.

We start iterating from the initial guess which exceeds twice the 'no-overflow' level, as shown in Fig.12(right) by a bold solid line, $k = 0$. This is done to ensure that the zoom domain Ω_2 is covered by water, i.e. non-trivial sensitivity information reaches the sensor at the first iteration. The solution obtained by the JAC algorithm is presented in Fig.12(right). Here, by a faint solid line, we show the reference BC and, by bold solid lines, the retrieved value after k iterations. The final solution for $k = 50$ is shown by a dashed line. One can see that the JAC algorithm allows us to identify satisfactorily the unknown inflow BC during the period $t \in [300 - 750]\,s$, i.e. when the inflow BC is large enough to cause a flood event (thus to be detected by sensor B). One cannot expect to identify the inflow BC at times preceding to this period, since the flow is confined by the main channel and no flow information is available. This example shows that the local 2D zoom model can play the role of an operator that maps local 2D data into the 1D-net global model; data which could not be assimilated if the global model alone is considered. This last feature of zoom models seems interesting for real applications. Usually, many observations are made during a flood event, but they cannot be assimilated since they cannot be represented by the 1.5D model.

8 Conclusion

Global models which consider large scale phenomena in full complexity everywhere are unlikely to be implemented because of present computational limitations. However, in some parts of a model domain the effects which are not represented by the global model become important and really should be taken into account. Hence, 'richer' local models may become of interest. Also, in the DA context, richer local

models may allow measured physical quantities to be assimilated which are not the variables of the global model. If the extra state variables of a 'richer' local model match with some of the measured quantities, it can be viewed as a mapping operator.
The application we consider in this paper is river hydraulics. The global model is an open-channel network model based on 1.5D flow models, i.e. models that use the 1D equations (St-Venant of SWE) with source terms. The expressions for these source terms are derived by empirical consideration. We seek to use the 2D SWE model in certain circumstances where and when the use of a 1.5D model is not sufficient, such as flood event, for example. For simplicity we assume that our 1.5D model is based on the 1D SWE.
We suggest the use of a zoom model (the two-way nested richer local model) superposed on an element of the global model. The boundary conditions for the zoom model are provided by the global model, while the zoom model provides a feedback in the form of defect correction via a source term. This arrangement is convenient because it allows modifications in the global model to be avoided. The zoom and 1.5D models are coupled using the WFR method. Numerical experiments on a simple hydrodynamic configuration have shown that 2-3 iterations of this procedure is enough to couple the models. The method is efficient for the case when the 2D flow at the boundaries of the 'zoom' model exhibits essentially 1D behavior.
Without DA, the global model and 'zooms' can be coupled using the WFR method. A possible difficulty is that these models are not consistent, in our case because of different dimensionality. In order to specify the BC of the zoom model one needs more information than the 1.5D model can provide. Therefore, additional a-priori assumptions must be used. However, if measured data are available, the coupling problem with DA actually becomes simpler. This is because the information needed for coupling is extracted from measured data. We formulate the generalized cost functional which includes both the standard data misfit functional and the coupling conditions in a weak integral form. This cost functional is minimized using the LBFGS method, while the gradient is computed using the adjoint of the one-way relaxed model. Therefore, we solve simultaneously the data assimilation and coupling problems as a single minimization problem. We call this approach a joint assimilation-coupling method (JAC). Numerical tests to verify the suggested method have been conducted. These experiments show that the method is feasible.
The basic ideas presented in this paper have been verified using a simple 'toy' configuration. The next developments for this method should be:
a) the use of a the 1.5D open channel flow model based on the St-Venant equations instead of the SWE;
b) the use of a non-uniform spatial mesh in the 2D zoom model, that will allow more realistic configurations to be modeled, such as curvilinear channels, river confluence points, etc.

Acknowledgments

The authors gratefully acknowledge the contribution of the following: Dr. J.B. Faure, CEMAGREF (Lyon) for useful discussions which helped to formulate the practical problem; Mr. M. Honnorat, LMC-IMAG (Grenoble) for his help in computational issues; Dr Graham Copeland, Department of Civil Engineering, University of Strathclyde for his help with the English language.

A Characteristic boundary conditions

In order to implement the 'zoom' model we have to consider the 2D local SWE model with open boundaries Γ_3, Γ_4, Γ_5 and Γ_6. Therefore, the theory of characteristics can be used [3] to define the BC. We note that the original problem (1) can be rewritten in the non-conservative form

$$U_t + \mathbb{A}U_x + \mathbb{B}U_y - S(U) = 0 \tag{A.1}$$

where

$$\mathbb{A} = \begin{pmatrix} 0 & 1 & 0 \\ c^2 - u^2 & 2u & 0 \\ -uv & v & u \end{pmatrix}, \quad \mathbb{B} = \begin{pmatrix} 0 & 0 & 1 \\ -uv & v & u \\ c^2 - u^2 & 0 & 2v \end{pmatrix}, \tag{A.2}$$

$c = (gh)^{1/2}$ is the celerity and $u = q/h$, $v = p/h$ are the mean velocities. As long as c, u, v are considered as given coefficients dependent on (x, y, t) only, the transport part of the equation (A.1) becomes linear and it can be reduced to a pseudo-canonical form

$$W_t + \Lambda W_x + R\mathbb{B}R^{-1}W_y - (R_t + \Lambda R_x)R^{-1}W - S(R^{-1}W) = 0 \tag{A.3}$$

where

$$W = RU, \quad \Lambda = \begin{pmatrix} u + c & 0 & 0 \\ 0 & u - c & 0 \\ 0 & 0 & u \end{pmatrix}, \quad R = \begin{pmatrix} c - u & 1 & 0 \\ -(c + u) & 1 & 0 \\ -v & 0 & 1 \end{pmatrix} \tag{A.4}$$

The variables $W = [w_1, w_2, w_3]^T$ are conventionally called 'characteristic' variables. Dependent on the sign of the corresponding eigenvalue in Λ they can be either

incoming or outgoing variables. A general rule to set up a well-posed open boundary problem is that one must specify the incoming characteristic variables only.

The representation (A.3)-(A.4) could be used to construct the open boundary BC, if the x-axis is the dominant incidence direction. At each boundary we choose the local dominant direction and construct the co-ordinate systems (x'_l, y'_l) rotated in respect to the original co-ordinate system by the angle $\beta_l,\ l = 3, 4, 5, 6$ as shown in Fig.A.1(left). For example, in the fluvial case the dominant characteristic direction is expected to be close to the tangent to the channel median curve. If we denote α the angle between x-axis and this tangent, then $\beta_3 = \alpha(x')|_{x'\in\Gamma_3}$ and $\beta_4 = 180^\circ + \alpha(x')|_{x'\in\Gamma_4}$. For boundaries Γ_5 and Γ_6 we can chose the dominant direction coincident with the inward normal to the boundary. Since the 2D SWE remain in the same form in any rotated co-ordinate system (x', y') where (q, p) are replaced by (q', p'), the representation (A.4) also remains in the same form. That is, in the sub-critical case $w_1(\Gamma_l, t)$ is the incoming characteristic variable to be imposed, $w_2(\Gamma_l, t)$ is the outgoing characteristic variable to be interpolated from the interior. The variable $w_3(\Gamma_l, t)$ can be either the incoming or outgoing variable dependent on the sign of u'_l.

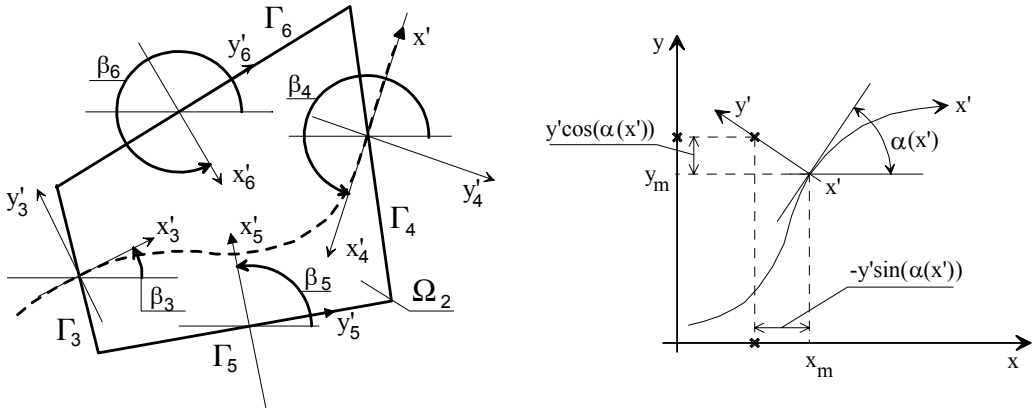

Fig. A.1. Left: domain Ω_2, its boundaries and orientation of auxiliary co-ordinates; Right: channel-following co-ordinates

B Rotated 1D main channel equations

Let us assume that the median curve of the main channel is specified in parametric form as follows

$$x_m = \phi_1(x'), \quad y_m = \phi_2(x')$$

We intend to consider the 2D SWE problem in the channel-following co-ordinates, thus we link the axis x' to the median curve. The axis y' is locally orthonormal to x'

as shown in Fig.A.1(right). The original co-ordinates of the point located at (x', y') in the channel-following co-ordinate system are

$$x = \phi_1(x') - y' sin(\alpha(x')), \quad y = \phi_2(x') + y' cos(\alpha(x'))$$

We differentiate both expressions on x and y as follows:

$$\begin{aligned} \frac{\partial x}{\partial x} &= \frac{\partial \phi_1}{\partial x'}\frac{\partial x'}{\partial x} - y' cos(\alpha)\frac{\partial \alpha}{\partial x'}\frac{\partial x'}{\partial x} - \frac{\partial y'}{\partial x} sin(\alpha) \equiv 1 \\ \frac{\partial y}{\partial x} &= \frac{\partial \phi_2}{\partial x'}\frac{\partial x'}{\partial x} - y' sin(\alpha)\frac{\partial \alpha}{\partial x'}\frac{\partial x'}{\partial x} + \frac{\partial y'}{\partial x} cos(\alpha) \equiv 0 \end{aligned} \tag{B.1}$$

$$\begin{aligned} \frac{\partial x}{\partial y} &= \frac{\partial \phi_1}{\partial x'}\frac{\partial x'}{\partial y} - y' cos(\alpha)\frac{\partial \alpha}{\partial x'}\frac{\partial x'}{\partial y} - \frac{\partial y'}{\partial y} sin(\alpha) \equiv 0 \\ \frac{\partial y}{\partial y} &= \frac{\partial \phi_2}{\partial x'}\frac{\partial x'}{\partial y} - y' sin(\alpha)\frac{\partial \alpha}{\partial x'}\frac{\partial x'}{\partial y} + \frac{\partial y'}{\partial y} cos(\alpha) \equiv 1 \end{aligned} \tag{B.2}$$

Taking into account that

$$\frac{\partial \phi_1}{\partial x'} = cos(\alpha); \quad \frac{\partial \phi_2}{\partial x'} = sin(\alpha)$$

we multiply equations (B.1) and (B.2) consequently by the rotation matrix (from the left)

$$\begin{pmatrix} cos(\alpha) & sin(\alpha) \\ -sin(\alpha) & cos(\alpha) \end{pmatrix}$$

and find the transformation coefficients as follows

$$\frac{\partial x'}{\partial x} = \frac{cos(\alpha)}{1 - y'\alpha_{x'}}, \quad \frac{\partial y'}{\partial x} = -sin(\alpha), \quad \frac{\partial x'}{\partial y} = \frac{sin(\alpha)}{1 - y'\alpha_{x'}}, \quad \frac{\partial y'}{\partial y} = cos(\alpha) \tag{B.3}$$

This co-ordinate transformation is well-posed and its inverse exists for any y' smaller than the curvature radius. If $y'\alpha_{x'}$ is reasonably small (that is often justified in fluvial applications) we can use the Taylor expansion to represent first and third coefficients in (B.3) as follows

$$\frac{\partial x'}{\partial x} = cos(\alpha)(1 + O(y'\alpha_{x'})), \quad \frac{\partial x'}{\partial y} = sin(\alpha)(1 + O(y'\alpha_{x'}))$$

The Jacobian of the transformation becomes $T(\alpha) + T_{curv}(\alpha)$, where

$$T(\alpha) = \begin{pmatrix} cos(\alpha) & -sin(\alpha) \\ sin(\alpha) & cos(\alpha) \end{pmatrix}, \quad T_{curv}(\alpha) = \begin{pmatrix} O(cos(\alpha)y'\alpha_{x'}) & 0 \\ O(sin(\alpha)y'\alpha_{x'}) & 0 \end{pmatrix}$$

Thus, one can write

$$\begin{bmatrix} \frac{\partial \cdot}{\partial x} \\ \frac{\partial \cdot}{\partial y} \end{bmatrix} = (T(\alpha) + T_{curv}(\alpha)) \begin{bmatrix} \frac{\partial \cdot}{\partial x'} \\ \frac{\partial \cdot}{\partial y'} \end{bmatrix} \tag{B.4}$$

The components of discharge in the original and channel-following co-ordinates are related by the rotation $T(\alpha)$

$$\begin{bmatrix} q \\ p \end{bmatrix} = T(\alpha) \begin{bmatrix} q' \\ p' \end{bmatrix} \tag{B.5}$$

We apply (B.4) and (B.5) to (1) and multiply by $T^T(\alpha)$ from the left the momentum equations in (1). Then, it is easy to ascertain that in the channel-following co-ordinates (x', y') the 2D SWE model comprises the principal part in the form (1), where (h, q, p) are replaced by (h, q', p'), and additional terms by order of magnitude $y'\alpha_{x'}$ related to the matrix $T_{curv}(\alpha)$, both in the continuity and momentum equations.

C Model error and inverse problem accuracy

Let us consider a linear inverse problem in the form

$$Au = \hat{f}$$

where u is a control, $\hat{f}$ are measurements and A is an operator which maps u to $\hat{f}$. In the identical twin experiment we generate the synthetic data using a fine grid solution, i.e.

$$\hat{f}_h = A_h u_h$$

where h is a 'fine mesh-size' used in A_h. Naturally, the solution of the fine grid inverse problem is

$$u_h = A_h^{-1} f_h = A_h^{-1} A_h u_h = u_h$$

i.e. it is exact. Now based on $\hat{f}_h$ we want to find the solution of the inverse problem formulated on coarse grid

$$A_H u_H = I_H^h \hat{f}_h$$

where H is a 'coarse mesh-size', A_H is a coarse grid operator, u_H is a coarse grid representation of control u_h, I_H^h is a restriction operator which maps f_h into the coarse grid representation f_H. The solution of the coarse-grid inverse problem is

$$u_H = A_H^{-1} I_H^h \hat{f}_h$$

This solution must be interpolated to the fine grid, so we get finally

$$\hat{u}_h = I_h^H u_H$$

where I_h^H is a prolongation operator. Next we compute the difference between $\hat{u}_h$ and u_h as follows:

$$\hat{u}_h - u_h = (I_h^H A_H^{-1} I_H^h A_h - I) u_h$$

where I is an identity operator. So, it is clear that the solution error norm depends on the norm of a 'grid inconsistency operator'

$$\Delta = I_h^H A_H^{-1} I_H^h A_h - I$$

It is clear that

$$\lim_{H \to h} ||\Delta|| = 0$$

However, as H deviates from h the norm of Δ grows. This is a grid inconsistency related 'model' error, which appears in our numerical example. Let us note, that another type of model error is called the 'representation' error. This error appears because the model does not represent all phenomena existing in nature, which generate actual (not synthetic) measurements. Some bounds for $||\Delta||$ given the particular form of the operator A and grid transfer operators I_h^H and I_H^h could be estimated. This is, however, quite a laborious independent task, which is beyond the scope of this paper.

References

[1] O.M. Alifanov, E.A. Artyukhin, S.V. Rumyantsev, *Extreme Methods for Solving Ill-Posed Problems with Applications to Inverse Heat Transfer Problems*, Begel House Publishers, (1996)

[2] E. Belanger and A. Vincent. *Data assimilation (4DVAR) to forecast flood in shallowwaters with sediment erosion*. Journal of Hydrology, 300(14) :114125 (2005).

[3] E. Blayo, L. Debreu *Revisiting open boundary conditions from the point of view characteristic variables*, Ocean Modelling, 9 (2005) 231-252

[4] A. Brandt, *Multi-level adaptive solutions to boundary-value problems*, Math. Comp., 31 (1977) 333-390

[5] Cunge, J.A., Holly, F.M., Verwey. A. *Practical Aspects of Computational River Hydraulics*. Pitman, London,(1980).

[6] L. Formaggia, J.F. Gerbeau, F. Nobile, A. Quarteroni, *On the coupling of 3D and 1D Navier-Stokes equations for flow problems in compliant vessels*, Comput. Methods Appl. Mech. Engrg., 191(2001) 561-582

[7] A.D. Fox, S.J.Maskell, *Two-way interactive nesting of primitive equation ocean models with topography*, Journal of Physical Oceanography, 25 (1995) 2977-2996

[8] M.J. Gander, L. Halpern, F. Nataf, *Optimal convergence for overlapping and non-overlapping Schwarz waveform relaxation*, Eleventh International Conference on Domain Decomposition Methods. C-H. Lai, P. Bjorstad, M.Cross, O. Widlund ed. (1999) 27-36

[9] I. Gejadze, M. Honnorat, X. Lai, J. Marin, J. Monnier. *Dassflow v2.0: a variational data assimilation software for river flows*. Research Report INRIA, february 2007. http://ljk.imag.fr/MOISE/dassflow

[10] I.Yu. Gejadze, G.J.M. Copeland, *Open boundary control problem for Navier-Stokes equations including a free surface: adjoint sensitivity analysis*, Comp. Math. with Appl., 52 (2006) 1269-1288

[11] P. Gervasio, J.L. Lions, A. Quarteroni, *Heterogeneous coupling by virtual control methods*, Numer. Math., 90 (2001) 241-264

[12] J.Ch. Gilbert, C. Lemarechal, *Some numerical experiments with variable storage quasi-Newton algorithms*, Mathematical Programming, 45 (1989) 503-528

[13] A. Hascoet, V. Pascual, TAPENADE 2.1 user's guide, Technical Report RT-300, INRIA, 2004

[14] M. Honnorat, J. Monnier, F-X Le Dimet *Lagrangian data assimilation for river hydraulics simulations*, Comp. Visu. Sc. To appear (2007).

[15] E. Lelarasmee, *The Waveform Relaxation Method for the Time Domain Analysis of Large Scale Nonlinear Dynamical Systems*, Ph.D. thesis, Univ. of California, Berkeley, 1982.

[16] Le Dimet, F.-X. and Mazauric, C. and Castaings, W. *Prospects for the use of data assimilation for flood prediction* Workshop on Flood Prevention and Control on the Yangtze River (FOCYR). (2004)

[17] E. Miglio, S. Perotto, F. Saleri, *Model coupling techniques for free-surface flow problems*, Part I, Proceedings of the Fourth World Congress of Nonlinear Analysis WCNA-2004, Orlando, Florida, USA (2004)

[18] V.A. Morozov *Methods for Solving Incorrectly Posed Problems*, Springer, (1984)

[19] E.F. Toro, *Shock-capturing methods for free-surface shallow flows*. J. Wiley and Sons (2001)

[20] R.J. Le Veque, *Balancing source terms and flux gradients in high-resolution Godunov methods: the quasi-steady wave propagation algorithm*, J. Comp. Physics, 146 (1998) 346-365